

OPEN ACCESS


IOP Publishing

Journal of Optics

J. Opt. 22 (2020) 115604 (7pp)

<https://doi.org/10.1088/2040-8986/abb990>

Reduction of response time in transmissive optically addressed spatial light modulator using solution-based ZnO NP/PEDOT:PSS heterojunction

Xin Chang¹ , Jin Li¹, Pawan Kumar Shrestha¹, Shunpu Li², Kasia Surowiecka¹ and Daping Chu¹ 

¹ Centre for Photonic Devices and Sensors, Department of Engineering, University of Cambridge, Cambridge, United Kingdom

² College of New Materials and New Energies, Shenzhen Technology University, Shenzhen, People's Republic of China

E-mail: dpc31@cam.ac.uk

Received 15 June 2020, revised 22 August 2020

Accepted for publication 17 September 2020

Published 8 October 2020



CrossMark

Abstract

An optically addressed spatial light modulator (OASLM) works by using the intensity of a 'write' light to modulate the phase of a 'read' light. OASLM using ZnO nanoparticles (NPs) as a photoconductor is important to holographic displays because of its record-high spatial resolution. However, its response time to the write light is long and the switch-off time (τ_{off}) can take tens of seconds due to the trap states in the ZnO NP layer. This results in residual images and poses limitations to its application in dynamic holographic displays. In this work, a ZnO NP photoconductor was replaced by a solution-processed ZnO NP/PEDOT:PSS heterojunction photodiode and the τ_{off} of OASLM was significantly reduced to about 0.6 s. Electrical and optical properties of the heterojunction were characterized and a barrier height of 0.604 eV was determined by CV measurement. The heterojunction-based OASLM was then fabricated and its light modulating performance was investigated by using a diffractive phase grating. Finally, impedance spectroscopy was used to analysis the device equivalent circuit and optimize the operation of the OASLM.

Supplementary material for this article is available [online](#)

Keywords: OASLM, ZnO NP, PEDOT:PSS, heterojunction, holography

(Some figures may appear in colour only in the online journal)



Original content from this work may be used under the terms of the [Creative Commons Attribution 4.0 licence](https://creativecommons.org/licenses/by/4.0/). Any further distribution of this work must maintain attribution to the author(s) and the title of the work, journal citation and DOI.

1. Introduction

Spatial light modulators (SLMs) have become the key component for digital holography (DH) and liquid crystal (LC)-based devices are among the most popular SLMs because of their versatile light modulation modes and relatively low cost [1, 2]. LC-based SLMs are addressed electrically by

pixels or optically by a write light with spatially varying intensity (OASLM). OASLM is normally less expensive and less complicated than electrically addressed SLM (EASLM). More importantly, OASLM has its unique advantages over EASLM for the application of holographic displays, such as the higher resolution, elimination of pixels and associated dead space between pixels, which results in a large viewing angle and less undesired diffraction patterns in the replay image. Moreover, large-size OASLM can be realized, which is crucial for high-resolution reconstruction. Several materials have been used as the photoconductor in OASLM, such as amorphous arsenic trisulfide ($a\text{-As}_2\text{S}_3$) [3], crystal silicon [4], and phthalocyanine [5]. ZnO nanoparticle (NP)-based OASLM using nematic LC has been reported to be capable of providing a highest-in-record resolution of 825 lp mm^{-1} due to the existence of trap states in the ZnO NP layer [6]. This is significant to achieve a large-size reconstruction image. However, the trap states in ZnO NP also lead to a long τ_{off} after UV is turned off, leaving a ‘ghost’ image (residual image) [7, 8]. The τ_{off} normally takes tens of seconds and it makes dynamic DH extremely challenging.

A PIN photodiode has been used for high-speed OASLM and its response time is mainly limited by the RC time constant [9–11]. For instance, binary OASLMs using PIN photodiode of hydrogenated amorphous silicon ($a\text{-Si:H}$) and ferroelectric LC was reported to have a response time of $155 \mu\text{s}$ and resolution of 40 lp mm^{-1} [12, 13]. Faster OASLM using smectic-A LC was also published and the response time was $40 \mu\text{s}$ at 29°C [14]. Higher resolution of 175 lp mm^{-1} was achieved using a similar OASLM structure, which has a response time of $70 \mu\text{s}$ and real-time holographic reconstruction was proposed with an operating frequency of up to 560 Hz [15]. However, PIN-based OASLMs generally have a low resolution due to lateral charge spreading (drift and diffusion in the bulk and at the interface) and electrical fringing field [16, 17]. Other methods were also reported for the improvement of the time response of LC-based devices, such as utilizing a surface-induced photorefractive effect [18] and introducing a gold film on one of the ITO electrodes [19].

In this paper, a solution-based heterojunction photodiode made with ZnO NP and PEDOT:PSS (poly(3,4-ethylenedioxythiophene)-polystyrenesulfonic acid) was reported. More importantly, a reduced τ_{off} of $\sim 0.65 \text{ s}$ was achieved in the ZnO NP/PEDOT:PSS heterojunction-based OASLM, which also displayed an improved diffraction efficiency (8.09%). PEDOT:PSS is a popular type of conductive polymer with high electrical conductivity, low absorption in the visible range and high stability in the air [20–22]. Recently, PEDOT:PSS has been used to form high-performance Schottky junctions with a single-crystal and amorphous ZnO thin film [23–26]. The junction between ZnO NP and PEDOT:PSS was also observed in this work and it was characterized in terms of electrical and optical properties (in the next section). The application of ZnO NP/PEDOT:PSS heterojunction in OASLM was then presented, following the detailed fabrication process of the heterojunction-based OASLM. Impedance

spectroscopy was also used to determine the resistance of each layer in order to optimize the operation. In the end, a fast-switching OASLM based on ZnO NP/PEDOT:PSS heterojunction was successfully demonstrated.

2. Characterization of ZnO NP/PEDOT:PSS heterojunction

The fabrication of the ZnO NP/PEDOT:PSS heterojunction was carried out at a relatively low temperature of 200°C . Firstly, PEDOT:PSS thin film was prepared by spin-coating (4000 rpm, 30 s) diluted PEDOT:PSS water suspension (Clevis PH-1000, 0.38 wt%) on pre-cleaned ITO glass substrate, followed by baking at 200°C for 1 h in air. Secondly diluted ZnO NP dispersion in ethanol (Sigma Aldrich Co., 75 mg ml^{-1}) was spin-coated (4000 rpm, 30 s) on top of the PEDOT:PSS thin film and left for baking at 200°C for 1 h in air. Finally, 100 nm aluminum (Al) was deposited on top as electrode by e-beam evaporation to form Ohmic contact [27]. The ZnO NP film was inspected by SEM (Zeiss LEO Variable Pressure) and AFM (DI3100), as is shown in figure 1(a) and its inset respectively. The size of ZnO NP is $<100 \text{ nm}$ and the average size is between $30\sim 50 \text{ nm}$, which was confirmed by dynamic light scattering (not shown). The mean surface roughness of the ZnO NP film was measured to be 5.8 nm by AFM measurement in the tapping mode over a $1 \mu\text{m} \times 1 \mu\text{m}$ area.

IV measurement was carried out for ZnO NP/PEDOT:PSS heterojunction and its rectification behaviour is illustrated in figure 1(b). The ‘On/Off’ current ratio ($I_{\text{on}}/I_{\text{off}}$) at 2 V is about 6.7×10^3 (in black). In contrast, the IV characteristics of Al-ZnO NP-ITO sample (in red) prepared under the same condition show no difference between positive and negative voltages. The junction barrier height was also determined at 100 Hz by CV measurement using Autolab PGSTAT302. The imaginary impedance ($Z_{\text{imaginary}}$) increases with increasing reversed-bias voltage (V_{reverse}) due to the widening of the depletion region, as is shown on the left of figure 1(c). The barrier height can be extracted by the intersection of $1/C^2$ with x -axis and its value was determined to be 0.604 eV . This is consistent with the published value for amorphous ZnO/PEDOT:PSS Schottky junction [25, 26].

The optical properties of the ZnO NP/PEDOT:PSS heterojunction were also investigated. Figure 1(d) shows the UV-visible spectroscopy of ZnO NP (in red) and heterojunction (in black), which indicates that the optical absorption over the visible range ($380 \sim 700 \text{ nm}$) is enhanced by introducing a PEDOT:PSS layer and more importantly, the wavelength for photoexcitation is not affected. Moreover, the UV response (405 nm , 0.76 mW cm^{-2}) was carried out, as shown in figure 1(e). A sandwiched sample of Al-ZnO-ITO was also measured as a comparison. It clearly demonstrates that the heterojunction has a shorter ‘fall’ time (τ_{fall}) of 11.4 s than ZnO NP (32.8 s), which has a long falling ‘tail’ and could severely prolong the τ_{off} of OASLM. Therefore, the fast switching-off

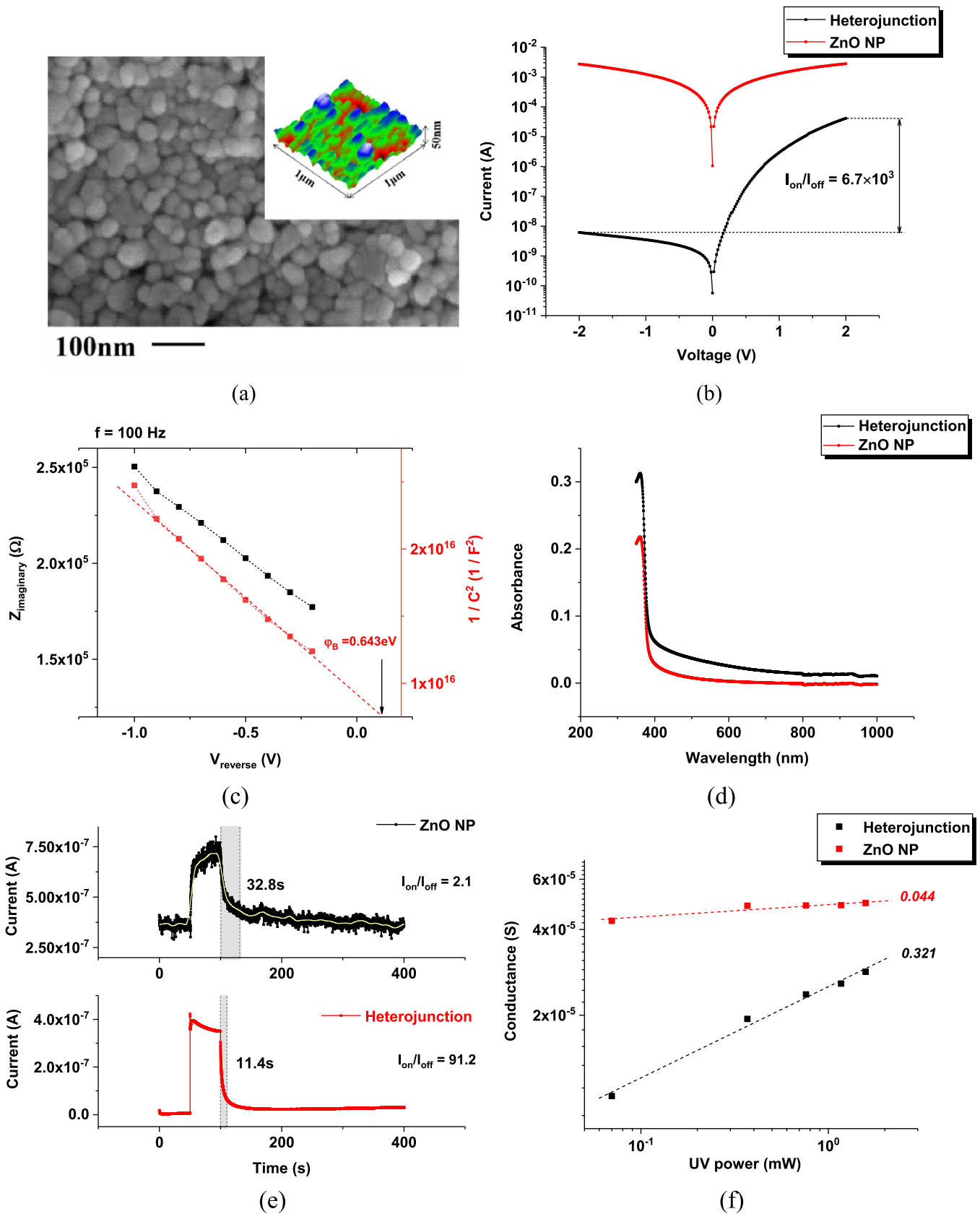


Figure 1. (a) SEM and AFM image of ZnO NP. (b) IV characteristics of ZnO NP/PEDOT:PSS heterojunction and ZnO NP. (c) Imaginary impedance under various reversed-bias voltage (black) and the extraction of barrier height by plotting $1/C^2$ (red). (d) Absorption spectrum of heterojunction and ZnO NP. (e) UV response of heterojunction and ZnO NP. (f) UV responsivity of heterojunction and ZnO NP.

of OASLM can be realized if it is switched off during the rapid decay of photocurrent rather than the ‘tail’. This is discussed in more details in the following section. Furthermore, the current gain of heterojunction (ΔI) is 91.2, which is higher than that of ZnO NP (2.1). The comparison in responsivity is also illustrated in figure 1(f). Electrical conductance is plotted against increasing UV power density (both in the Log scale) and the slope for the heterojunction is extracted to be 0.321, compared to 0.044 of ZnO NP. Therefore, it can be concluded that the heterojunction photodiode has a better optical performance than ZnO NP photoconductor in terms of response time, current gain and responsivity.

3. Fabrication and optimization of heterojunction-based OASLM

The fabrication of heterojunction-based OASLM is similar to the process described in the previous section. After the heterojunction was prepared on ITO glass, a thin layer of SiO₂ (50 nm) was deposited on the top by e-beam evaporation to minimize the charge trapping at the interface. Another ITO glass covered with alignment layer after rubbing (prepared by spin-coating AL1254 polyimide at 3000 rpm for 50 s, followed by prebaking at 80 °C for 10 min and baking at 200 °C for 30 min) was brought into contact after the spacer (5 μm)/glue mixture was dispensed. The cell was then left in UV for curing (3 min) and nematic LC (MDA 981602) was fed into the cell gap at 90 °C by capillary force. The cell was then sealed by glue and left in UV for another 3 min. The structure of heterojunction-based transmissive OASLM is illustrated in figure 2(a).

The optical characterization of the OASLM was conducted using the setup in figure 2(b). The ‘4f’ (focal length = 150 mm) optical configuration was used to write a binary amplitude grating (150 lp mm⁻¹) onto the OASLM using a write light (405 nm) and the first-order diffraction pattern of the polarized ‘read’ light (635 nm) was used to analyse the light modulating performance. The low-resolution grating was used because the OASLM has a longer τ_{off} in this case. An aperture was located behind the OASLM to block the zeroth and higher-order patterns, and a photodetector was used to record the first-order diffraction pattern. The OASLM was driven by a function generator and an oscilloscope was used to synchronously record the driving signal and first-order signal. Initially, a sinusoidal wave with a peak amplitude (V_p) of 2 V and frequency (f) of 0.5 Hz was used to drive the OASLM. A sinusoidal driving signal can provide a higher diffraction efficiency compared to other driving signals such as triangular signal and square signal [28]. In addition, OASLM driven by a sinusoidal signal has negligible charging and discharging effect, which causes degradation of phase grating if a square driving signal is used. This is substantiated by simulation and experiments shown in the supplementary information (available online at <https://stacks.iop.org/JOPT/22/115604/mmedia>). The recorded signals are shown in figure 2(c) and the peaks in the first-order signal (last ~ 0.27 s) signify the phase grating in OASLM. It clearly shows that the OASLM only functions as a diffractive

grating when the heterojunction is reversely biased while the grating disappears if it is forward-biased. This is due to the high current gain when the heterojunction is under reversed bias, which leads to a large contrast in phase shift (δ) between adjacent grating levels ($\Delta\delta$) due to LC rotation, and hence a functioning phase grating. On the contrary, the $\Delta\delta$ is almost identical if the heterojunction is under forward bias because of the high ‘on’ current (I_{on}), which results in negligible diffraction. In addition, the diffraction efficiency (η) in this case was calculated to be 4.39%, which is improved compared to ZnO NP-based OASLM (<2%) [6]. First-order diffraction efficiency was used here to indicate the quality of the gratings written on the OASLM and it was determined by the ratio of the measured first-order intensity and zeroth-order intensity (without write light). It was also found that the diffraction efficiency was dependent on V_p and f of the driving signal, as shown in figures 2(d) and (e) respectively. It is evident that there is an optimal driving condition ($V_p = 1.9 \sim 2.0$ V, $f = 0.5 \sim 0.6$ Hz) with the highest diffraction efficiency for heterojunction-based OASLM.

The switch-off characteristics were also investigated, and the result is shown in figure 2(f). It takes about 1.8 s for the first-order signal to drop by 64.7% of its step height (maximum value—minimum value) after the write light is switched off and it takes a longer time to further decay to its minimum value (‘tail’). In comparison, a ZnO NP-based OASLM was fabricated under the same condition and it takes about 17 s to drop by the same proportion. It is also evident that the switch-off characteristics of the heterojunction-based OASLM is worse than that of the heterojunction itself (‘tail’ effect in particular) because of the impedance mismatching. Therefore, impedance spectroscopy was used to determine the resistance values for LC and the heterojunction individually in order to optimize the operation. A 5 μm thick LC cell (ITO-LC-ITO, 12 mm × 12 mm) was fabricated and its impedance spectroscopy (1 Hz~MHz) was measured at 2 V by Autolab PGSTAT302. The Nyquist plot is shown in figure 3(a) and its resistance ($R_{\text{LC}} = 50.8$ MΩ)/capacitance ($C_{\text{LC}} = 1.94$ nF) values were calculated by curve fitting. In order to determine the threshold voltage (V_{th}) for LC, $Z_{\text{imaginary}}$ of the cell was measured at 100 Hz under increasing DC voltages (V_{DC}) from 0 V to 4.5 V, as shown in figure 3(b). It shows that the $Z_{\text{imaginary}}$ starts to decrease when $V_{\text{DC}} > 0.5$ V because LCs rotate along the electric field and the dielectric constant effectively increases. Moreover, $Z_{\text{imaginary}}$ saturates when V_{DC} reaches ~2.0 V, indicating that most LCs are aligned with the electric field. Measurement was repeated on ZnO NP/PEDOT:PSS heterojunction at zero bias and the result is shown in figure 3(c). The resistance ($R_{\text{heterojunction}}$) was calculated to be 370 MΩ in dark conditions, which is consistent with the IV measurement and UV response in figures 1(b) and (e). The capacitance ($C_{\text{heterojunction}}$) was also plotted against increasing V_{reverse} from 0 V to -1 V (figure 3(d)) and it demonstrates that the junction capacitance decreases as V_{reverse} increases due to a wider depletion region. The plateau in capacitance might be caused by interface states or fitting error. Similarly, the resistance of the

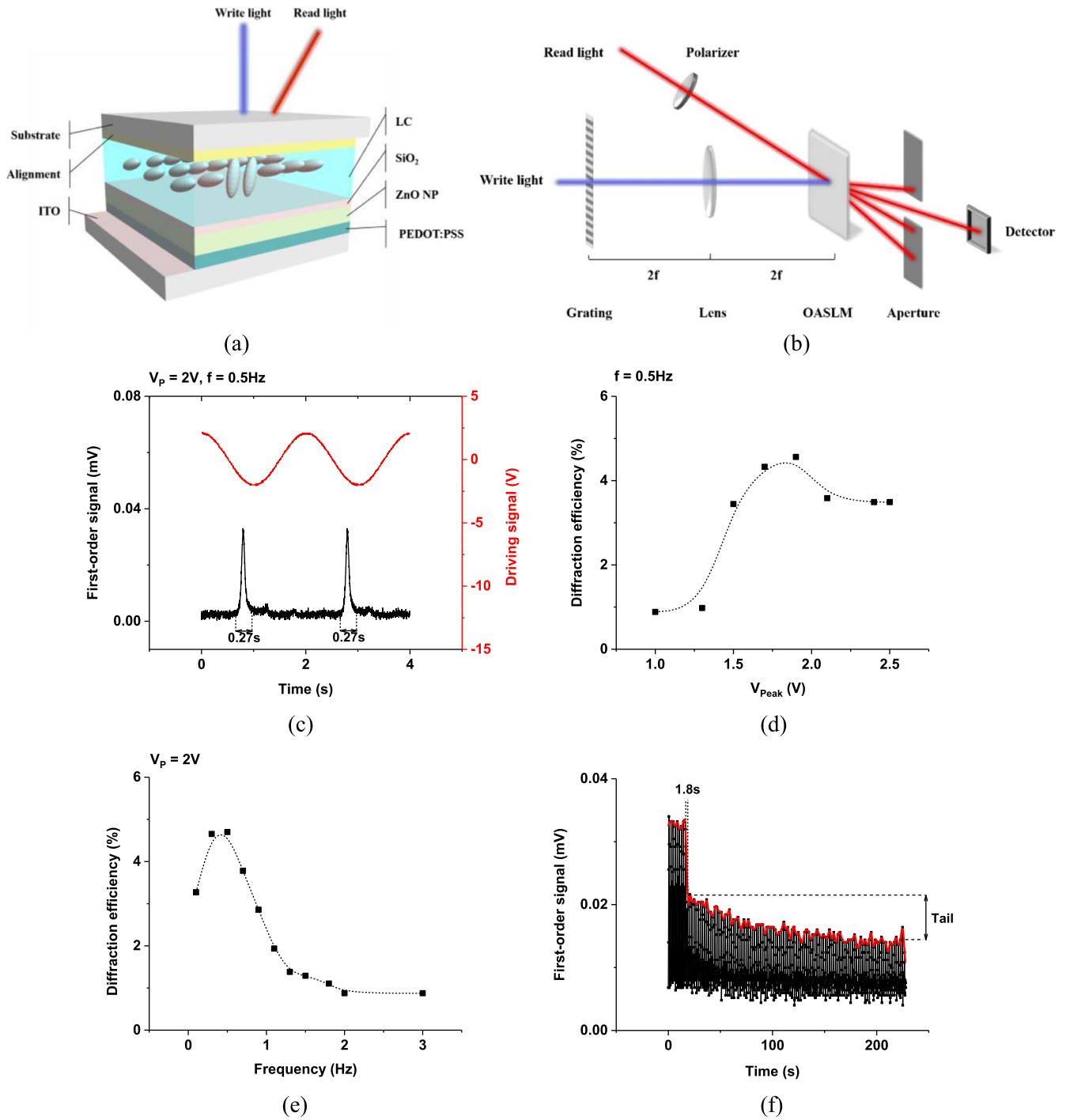


Figure 2. (a) An illustration of heterojunction-based OASLM. (b) The setup for optical characterization. (c) The driving signal and first-order signal when peak voltage amplitude is 2 V and frequency is 0.5 Hz. The effect of peak amplitude (d) and frequency (e) on diffraction efficiency. (f) Switch-off characteristics after the write light was turned off.

heterojunction under UV (1.58 mW cm^{-2}) was measured to be $35.2 \text{ K}\Omega$, decreased by $>10^4$ times compared to the dark resistance.

In order to restore LC after the UV was turned off, the voltage across LC needs to be $<0.5 \text{ V}$ (figure 3(b)), which indicates that the condition of $R_{\text{heterojunction}} > 150 \text{ M}\Omega$ needs to be met (V_p is maintained at 2 V). If the resistance of the alignment layer and passivation layer (SiO_2) is considered, the

condition for LC to switch back is $R_{\text{heterojunction}} \gg 150 \text{ M}\Omega$. Accordingly, OASLM is effectively switched off near the ‘tail’ of I_{photo} and this explains the decaying ‘tail’ of the first-order signal in figure 2(f). A schematic illustration is drawn in figure 3(e). The ‘near-tail switching’ can be significantly improved by decreasing the R_{LC} and the resistance of SiO_2 such that the LCs are restored at a smaller $R_{\text{heterojunction}}$. This was verified by fabricating an OASLM with $2 \mu\text{m}$ spacer and

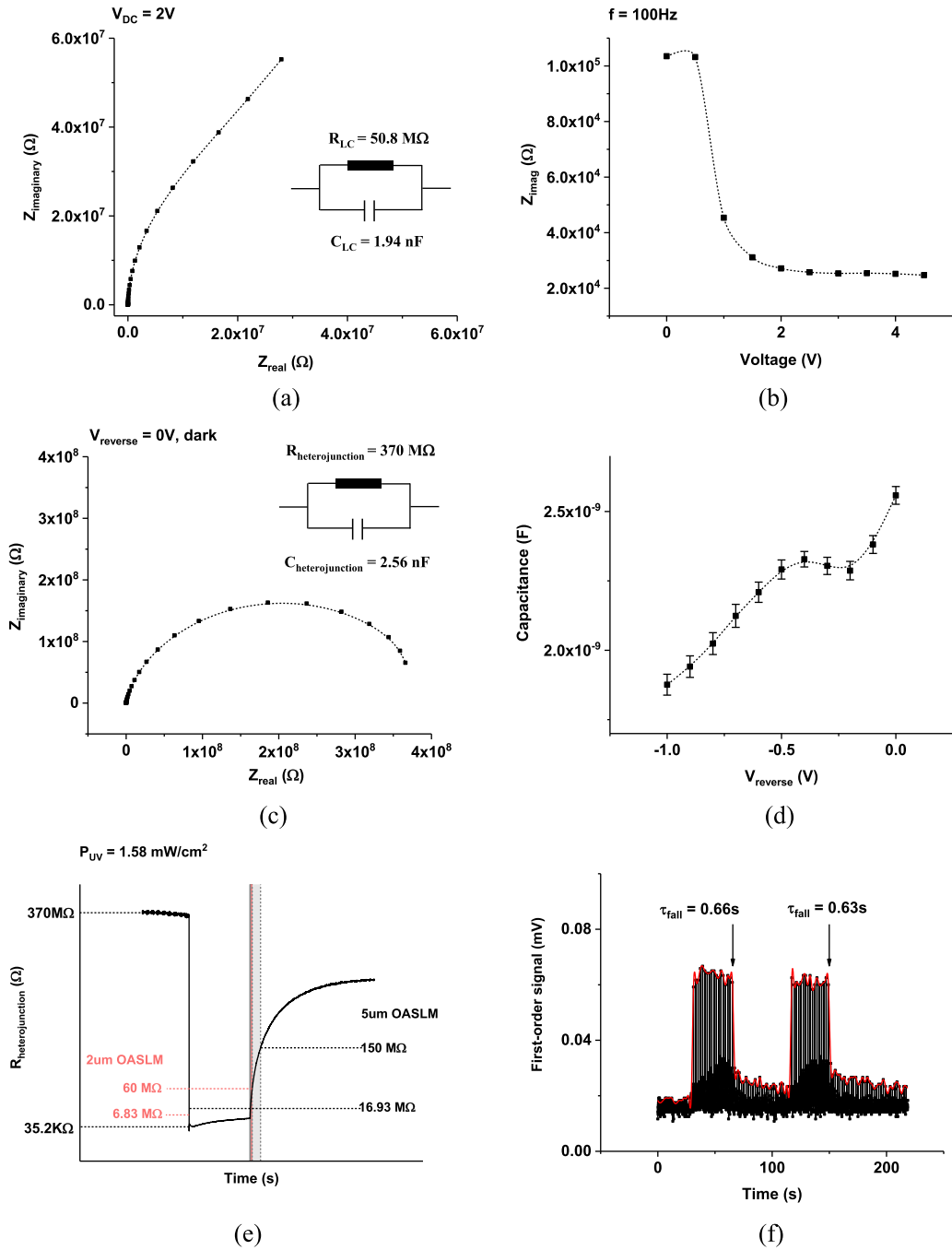


Figure 3. (a) The Nyquist plot of 5 μm LC cell when DC voltage is 2 V. (b) Determining the threshold voltage of LC by the change in imaginary impedance from 0 V to 4.5 V. (c) The Nyquist plot of ZnO NP/PEDOT:PSS heterojunction. (d) The change in heterojunction capacitance as reversed-bias voltage increases. (e) A schematic illustration of the switch-off process for 2 μm and 5 μm OASLM. (f) The switching operation of optimized OASLM with 2 μm in cell gap and 15 nm thick SiO_2 .

15 nm SiO_2 layer. As a theoretical estimation, LC starts to restore itself when $R_{\text{heterojunction}}$ is $<60 \text{ M}\Omega$ in this case. The switching response of the 2 μm thick OASLM was measured and the τ_{off} was measured to be 0.65 s (signal drops from 90% to 10% of its step height), as is shown in figure 3(f). In addition, it was also observed that the diffraction efficiency was improved to 8.09%, almost twice the value of 5 μm thick OASLM. This is also ascribed to the smaller $R_{\text{heterojunction}}$ required to switch off LC. Figure 3(e) also shows the maximum $R_{\text{heterojunction}}$ under UV in order to switch ‘on’

the LC and the 2 μm OASLM requires a lower $R_{\text{heterojunction}}$ (6.83 $\text{M}\Omega$) than 5 μm OASLM (16.93 $\text{M}\Omega$), which indicates that a higher UV power density is required for the thinner OASLM.

4. Conclusion

A fast-switching OASLM using ZnO NP/PEDOT:PSS heterojunction was successfully fabricated and its operation


in transmission mode was presented in this paper. Electrical and optical properties of the solution-based heterojunction were characterized. The barrier height was determined to be 0.643 eV and its optical performance shows a high responsivity and current gain (~ 91.2). The heterojunction was then used to fabricate OASLM and its light modulating behaviour was characterized by writing a diffractive phase grating on OASLM. A layer-by-layer analysis was carried out by impedance spectroscopy and a fast τ_{off} of ~ 0.65 s was achieved. A thinner LC layer and SiO₂ layer were used in order to better utilize the fast-switching characteristics of the ZnO NP/PEDOT:PSS heterojunction photodiode. As a result, a fast-switching OASLM with an enhanced diffraction efficiency of 8.09% was realized.

Acknowledgments

We thank the financial support of UK Engineering and Physical Sciences Research Council (EPSRC) through the EPSRC Centre for Doctoral Training in Integrated Photonic and Electronic Systems (Grant No. EP/L015455/1). X C thanks the China Scholarship Council for PhD studentship funding.

ORCID iDs

Xin Chang  <https://orcid.org/0000-0001-6408-765X>

Daping Chu  <https://orcid.org/0000-0001-9989-6238>

References

- [1] Lazarev G, Hermerschmidt A, Krüger S and Osten S *et al* 2012 LCOS spatial light modulators: trends and applications *Optical Imaging and Metrology: Advanced Technologies* 1st edn, ed W Osten and N Reingand (Weinheim: Wiley) pp 1–29
- [2] Bleha W P Jr and Lei L A 2013 Advances in liquid crystal on silicon (LCOS) spatial light modulator technology *Proc. SPIE* **8736** 87360A
- [3] Kirzhner M G, Klebanov M, Lyubin V, Collings N and Abdulhalim I 2014 Liquid crystal high-resolution optically addressed spatial light modulator using a nanodimensional chalcogenide photosensor *Opt. Lett.* **39** 2048
- [4] Efron U, Grinberg J, Braatz P O, Little M J, Reif P G and Schwartz R N 1985 The silicon liquid-crystal light valve *J. Appl. Phys.* **57** 1356–68
- [5] Collings N, Wilkinson T D, Jeziorska A, Davey A B, Movaghar B and Crossland W A 2004 Charge-injecting layers for liquid crystal light valves *Proc. SPIE* **5464** 421–7
- [6] Shrestha P K, Chun Y T and Chu D 2015 A high-resolution optically addressed spatial light modulator based on ZnO nanoparticles *Light Sci. Appl.* **4** e259
- [7] Barbier P R, Wang L and Moddel G 1993 Thin-film photosensor design and fabrication issues for liquid-crystal spatial-light modulators *Proc. SPIE* **2022** 98–110
- [8] Barbier P R, Wang L and Moddel G 1993 Thin-film photosensor design for liquid crystal spatial light modulators *Opt. Eng.* **33** 1322–9
- [9] Barbier P R and Moddel G 1992 Hydrogenated amorphous silicon photodiodes for optical addressing of spatial light modulators *Appl. Opt.* **31** 3898–907
- [10] Bowman S R, Rabinovich W S, Beadie G and Kirkpatrick S M 1998 Characterization of high performance integrated optically addressed spatial light modulators *J. Opt. Soc. Am. B* **15** 640–7
- [11] Collings N, Mias S, Wilkinson T D, Travis A R L, Moore J R and Crossland W A 2004 Optically addressed spatial light modulator: performance and applications *Proc. SPIE* **5213** 1–9
- [12] Li W, Rice R A, Moddel G, Pagano-Stauffer L A and Handschy M A 1989 Hydrogenated amorphous-silicon photosensor for optically addressed high-speed spatial light modulator *IEEE Trans. Electron Devices* **36** 2959–64
- [13] Moddel G, Johnson K M, Li W, Rice R A, Pagano-Stauffer L A and Handschy M A 1989 High-speed binary optically addressed spatial light modulator *Appl. Phys. Lett.* **55** 1–4
- [14] Abdulhalim I, Moddel G and Johnson K M 1989 High-speed analog spatial light modulator using a hydrogenated amorphous silicon photosensor and an electroclinic liquid *Appl. Phys. Lett.* **55** 1–4
- [15] Fukushima S, Kurokawa T and Ohno M 1991 Real-time hologram construction and reconstruction using a high-resolution spatial light modulator *Appl. Phys. Lett.* **58** 787–9
- [16] Wang L and Moddel G 1994 Effects of charge spreading on resolution of optically addressed spatial light modulators *Opt. Lett.* **19** 2033–5
- [17] Wang L and Moddel G 1995 Resolution limits from charge transport in optically addressed spatial light modulators *J. Appl. Phys.* **78** 6923–35
- [18] Pagliusi P and Cipparrone G 2004 Photorefractive effect due to a photoinduced surface-charge modulation in undoped liquid crystals *Phys. Rev. E* **69** 61708
- [19] Bugaychuk S *et al* 2020 Faster nonlinear optical response in liquid crystal cells containing gold nano-island films *Appl. Nanosci.* **28** 1
- [20] Nardes A M, Kemerink M and Janssen R A J 2007 Anisotropic hopping conduction in spin-coated PEDOT:PSS thin films *Phys. Rev. B* **76** 085208
- [21] Nardes A M *et al* 2007 Microscopic understanding of the anisotropic conductivity of PEDOT:PSS thin films *Adv. Mater.* **19** 1196–200
- [22] Sangeeth C S S, Jaiswal M and Menon R 2009 Correlation of morphology and charge transport in poly(3,4-ethylenedioxythiophene)-polystyrenesulfonic acid (PEDOT-PSS) films *J. Phys.: Condens. Matter.* **21** 072101
- [23] Nakano M *et al* 2007 Schottky contact on a ZnO (0001) single crystal with conducting polymer *Appl. Phys. Lett.* **91** 2005–8
- [24] Nakano M *et al* 2008 Transparent polymer Schottky contact for a high performance visible-blind ultraviolet photodiode based on ZnO Transparent polymer Schottky contact for a high performance visible-blind *Appl. Phys. Lett.* **93** 98–101
- [25] Sharma B K, Khare N and Ahmad S 2009 A ZnO/PEDOT:PSS based inorganic/organic heterojunction *Solid State Commun.* **3** 771–4
- [26] Hernandez-Como N, Rivas-Montes G, Hernandez-Cuevas F J, Mejia I, Molinar-Solis J E and Aleman M 2015 Ultraviolet photodetectors based on low temperature processed ZnO/PEDOT:PSS Schottky barrier diodes *Mater. Sci. Semicond. Process.* **37** 14–18
- [27] Jin Y, Wang J, Sun B, Blakesley J C and Greenham N C 2008 Solution-processed ultraviolet photodetectors based on colloidal ZnO nanoparticles *Nano Lett.* **8** 1649–53
- [28] Chang X, Shrestha P K and Chu D 2020 Reduction of switching time in ZnO nanoparticle-based reflective OASLM for holographic displays *Proc. SPIE* **11353** 113530M